UPPER SURFACE NACELLE INFLUENCE ON SCAR AERODYNAMIC CHARACTERISTICS AT TRANSONIC SPEEDS

Charles E. Mercer and George T. Carson, Jr.
NASA Langley Research Center

SUMMARY

An investigation has been conducted in the Langley 16-foot transonic tunnel to determine the influence of upper surface nacelles on the aerodynamic characteristics of a SCAR configuration at Mach numbers from 0.6 to 1.2. The arrow-wing transport configuration with detached engines located over the wing to produce upper surface exhaust flow effects was tested at angles of attack from -4° to 8° and jet total-pressure ratios from 1 (jet off) to approximately 10. Wing tip leading edge flap deflections of -10° to 10° were tested with the wing-body configuration only (no nacelles). Tests were made with various nacelle chordwise, spanwise, and vertical height locations over the Mach number, angle of attack, and jet total-pressure ratio ranges. The results show that deflecting the wing tip leading edge flap from 0° to -10° increased maximum lift to drag ratio by 1.0 at subsonic speeds. Installation of upper surface nacelles (no wing/nacelle pylons) increased the wing-body pitching moment at all Mach numbers and decreased the drag of the wing-body configuration at subsonic Mach numbers. Jet exhaust interference effects were negligible.

INTRODUCTION

Extensive research programs have been conducted to define and meet the design requirements of a commercially acceptable supersonic cruise transport aircraft. The highly swept arrow-wing supersonic transport configuration with engine nacelles mounted under the wing has been shown to be aerodynamically efficient at transonic and supersonic speeds. However, this type configuration exhibits poor takeoff and landing performance (refs. 1-4). Tests conducted in low speed wind tunnels have shown that blowing the jet exhaust over the upper surface of the wing provides an effective means for providing the high lift required for improved takeoff and landing performance (ref. 5).

The purpose of the present investigation was to determine the influence of upper surface nacelle exhaust flow on the longitudinal aerodynamic characteristics of a SCAR configuration at transonic speeds. The tests were conducted in the Langley 16-foot transonic tunnel at Mach numbers up to 1.2 and angles of attack from -4° to 8°. Jet total-pressure ratio was varied from 1 (jet off) to approximately 10. Three different chordwise, spanwise, and vertical height locations of the nacelles were investigated.

SYMBOLS

b	wing span
C_D	drag coefficient, Drag/qS
C_L	lift coefficient, Lift/qS
C_m	pitching-moment coefficient, Pitching moment/$qS\bar{c}$
C_p	pressure coefficient, $\frac{\Delta p}{q}$
c	local geometric chord of wing at any given spanwise location
$\bar{c}$	mean geometric chord of reference wing
D_e	nozzle exit diameter
L/D	lift to drag ratio
M	free-stream Mach number
NPR	nozzle pressure ratio
p	local static pressure
q	free-stream dynamic pressure
S	reference wing area
x	axial distance from wing leading edge to nacelle exit at any given spanwise station
y	lateral distance from body center plane to nacelle center plane perpendicular to body center plane
z	vertical height of nacelle centerline relative to wing leading edge at given spanwise station
α	angle of attack of model reference line
δ_F	wing-tip flap deflection angle relative to model reference line (positive leading edge up)
Δp	local static pressure minus free-stream static pressure

APPARATUS AND METHODS

Wind Tunnel

The 16-foot transonic tunnel, which has an octagonal test section with eight longitudinal slots, is an atmospheric wind tunnel with continuous air exchange for cooling. It has a remotely controlled Mach number range from 0 to 1.3. The average Reynolds number per meter varies from 9.71×10^6 at $M = 0.5$ to 12.6×10^6 at $M = 1.3$.

Model Description

A photograph of the model installed in the tunnel test section is shown in figure 1. A sketch of the SCAR model and air-powered sting system is presented in figure 2(a). A three-view computerized sketch showing nacelle reference planes is shown in figure 2(b). The model consisted of an arrow-wing-body combination having an overall length of 141.61 cm and a wing span of 84.66 cm. The fixed wing was highly swept back, twisted, and cambered with reflexed trailing edge. The main wing section has a leading edge sweep of 75° and the wing tips were swept 60°. The wing tips were detachable from the main wing. Wing tips were available with both positive and negative leading edge flap deflections. Twin vertical tails were located near the main wing/wing-tip juncture. Two engine nacelles were pylon-mounted over the wing as shown in figure 2(a). The engine nacelles were not attached to the wing-body configuration and no wing/nacelle pylon was provided to simulate this attachment. The nacelle geometry was configured to simulate a turbofan-jet engine operating in an afterburning-power mode. The nacelle support was designed to independently support the two nacelles above the wing-body configuration while providing the capability to vary the location of each nacelle relative to the configuration. The support system also provided the means for supplying high-pressure air to each engine nacelle.

Instrumentation and Data Reduction

Aerodynamic forces and moments on the wing-body configuration were measured with a six-component internal strain gage balance. Forces and moments on the nacelles were not measured for these tests. The upper surface of the left wing and lower surface of the right wing were pressure-instrumented with static pressure orifices. To insure a turbulent boundary layer over the wing-body configuration and nacelles, transition trips were applied to each of these components.

This investigation generally covered a Mach number range from 0.6 to 1.2. Angle of attack was varied from -4° to 8° and jet total-pressure ratio was varied from 1 (jet off) to approximately 10 depending on Mach number.

RESULTS

Wing-Tip Leading Edge Flap Effects

Presented in figure 3 are the effects of deflection of wing tip leading edge flaps on lift to drag ratio. These effects are for the wing-body configuration only without the influence of the nacelles. Lift to drag ratio as a function of lift coefficient is shown only for Mach 0.9. Similar results were obtained for other Mach numbers. Maximum lift to drag ratio occurs at a lift coefficient of 0.15 at all Mach numbers. Also shown in figure 3 is the variation of maximum lift to drag ratio as a function of flap angle for M = 0.6, 0.9, and 1.2. Leading edge flap deployment from 0° to -10° (leading edge down) increased maximum L/D by 1.0 at subsonic Mach numbers and by 0.5 at M = 1.2. This increase in $(L/D)_{max}$ is primarily a result of increased lift on the wing tips since other data, which are not presented in this report, show no significant effect on drag or pitching moment due to flap deflection.

Nacelle Installation Interference Effects

Aerodynamic force and moment characteristics of the wing-body configuration with and without interference effects due to nacelle installation (jet off) are presented in figure 4. Data are presented for Mach numbers of 0.9 and 1.2 which represent subsonic cruise and low supersonic flight conditions; data at M = 0.9 are typical of other subsonic Mach numbers. The unstable pitching moment coefficient, shown in figure 4, results from the model not having the horizontal and vertical tails which are required to balance the longitudinal loads of the aircraft (reference 1). Nacelle installation effects increased the wing-body pitching moment at all Mach numbers investigated. Installation of the over-the-wing nacelles reduced wing-body drag at subsonic speeds, but increased drag at M = 1.2. Little effect of nacelle installation was observed on airplane lift.

Figure 5 presents typical wing pressure distributions with and without the presence of the nacelles (jet off). Pressure coefficients are presented for Mach numbers of 0.9 and 1.2 and angles of attack of 0 and 4 degrees. Wing pressures in the proximity of the jet nacelles appear to be more positive over both the upper and lower surfaces of the wing at M = 0.9. Although the nacelle/support installation influenced the upper and lower wing surfaces at subsonic speeds, little effect due to the nacelle/support installation was observed on the wing lower surface pressure at M = 1.2.

The effect of jet operation on the SCAR aerodynamic characteristics is presented in figure 6 for M = 0.9 and M = 1.2. Jet exhaust flow was varied from jet off conditions (NPR $\approx$ 1) up to a jet total-pressure ratio of about 10. Jet interference effects on the wing appear to be negligible at all Mach numbers and nacelle locations investigated. This result indicates that the jet plume did not wash the wing upper surface and that there was no overall alteration of the wing flow field due to jet operation. Pressure distributions, shown in figure 7, show pronounced local effects from jet

operation (see y/(b/2) = 0.450 and 0.555 in figure 7(a) for example). These pressure perturbations appear to be self-compensating, however, such that little effect of jet operation occurs in the total wing-body forces and moments as shown in figure 6.

Nacelle Chordwise Location

The effect on the longitudinal aerodynamic coefficients due to chordwise movement of the nacelles (along the wing semispan station y/(b/2) = 0.46) is presented in figure 8. A chordwise nacelle location near the wing leading edge (x/c = -0.17 and 0.10) had little or no effect on the wing-body force and moment coefficients. However, as the jet nacelle approaches the wing trailing edge (x/c = 0.82), an increase in lift and a corresponding stabilizing effect on pitching moment are seen to occur at subsonic speeds. This indicates that a nacelle location near the wing trailing edge results in a beneficial influence on the wing flow field. However, as a result of increased drag, maximum lift to drag ratio was decreased by 1.0 at subsonic speeds when the nacelle was located near the wing trailing edge. At M = 1.2, nacelle chordwise location had generally smaller effects on wing-body forces and moments and has a negligible effect on lift to drag ratio.

Nacelle Spanwise and Vertical Location Effects

Shown in figures 9 and 10 are the effects of nacelle spanwise and vertical height locations on the wing-body longitudinal aerodynamic characteristics for Mach numbers of 0.9 and 1.2. Neither lateral or vertical movement of the jet nacelles had any significant influence on the wing-body force or moment coefficients. Examination of wing pressure distributions (not shown herein) indicates that either lateral or vertical movement of the jet nacelles resulted in localized pressure gradients with self-compensating effects on forces and moments.

Comparison With Theory

Comparisons between the experimental pressure coefficients on the wing and those predicted by the method of Woodward (reference 6) are shown on figure 11 for a Mach number of 0.9. Comparison appears to be poor mainly due to theory not accounting for vortex flow which apparently is forming on wing leading edge.

The predicted lift curve slope is similar to the measured values but at a slightly higher level as shown by figure 12.

CONCLUDING REMARKS

An investigation has been conducted in the Langley 16-foot transonic tunnel to determine the influence of upper surface nacelles on a supersonic cruise aircraft at Mach numbers up to 1.2. Results from this study indicate the following:

1. Wing tip leading edge flap deployment of -10° increased maximum lift to drag ratio by 1.0 at subsonic speeds.

2. Upper surface nacelle installation effects increased the wing-body pitching moment at all Mach numbers and decreased drag at subsonic Mach numbers. Jet exhaust interference effects were negligible at all conditions tested.

3. At subsonic speeds, chordwise movement of the over-the-wing nacelles, from a forward to an aft location, resulted in increased lift but a reduction of lift to drag ratio as a result of increased drag.

4. Spanwise and vertical nacelle position had negligible effects on wing-body aerodynamic characteristics.

REFERENCES

1. Morris, Odell P.; and Fournier, Roger H.: Aerodynamic Characteristics at Mach Numbers 2.30, 2.60, and 2.96 of a Supersonic Transport Model Having a Fixed, Wrapped Wing. NASA TM X-1115, 1976.

2. Harris, Roy V., Jr.; and Corlett, William A.: Transonic Aerodynamic Characteristics of a Supersonic Transport Model with Variable-Sweep Auxiliary Wing Panels, Outboard Tail Surfaces, and a Design Mach Number of 2.6. NASA TM X-1075, 1976.

3. Henderson, William P.: Low-Speed Aerodynamic Characteristics of a Supersonic Transport Model with a Highly Swept, Twisted and Cambered, Fixed Wing. NASA TM X-1249. 1966.

4. Henderson, William P.: A Low-Speed Longitudinal Stability Improvement Study on a Highly Swept Supersonic Transport Configuration. NASA TM X-1071, 1965.

5. Shivers, James P.; McLemore, H. Clyde; and Coe, Paul L., Jr.: Low-Speed Wind-Tunnel Investigation of a Large-Scale Advanced Arrow Wing Supersonic Transport Configuration With Engines Mounted Above the Wing for Upper-Surface Blowing. NASA TN D-8350, 1976.

6. Woodward, F. A.: An Improved Method for the Aerodynamic Analysis of Wing-Body-Tail Configuration in Subsonic and Supersonic Flow. NASA CR-2228, May 1973.

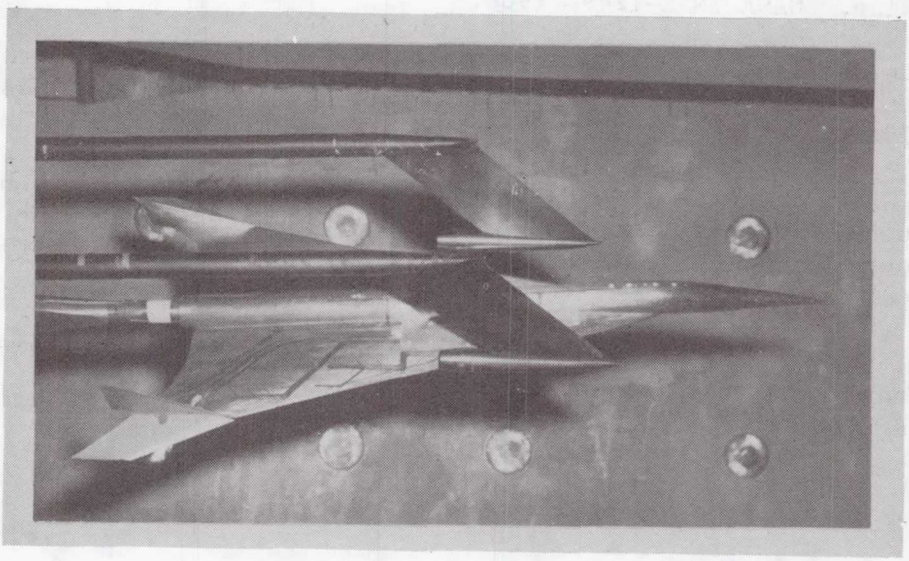

Figure 1.- Model in Langley 16-foot transonic tunnel.

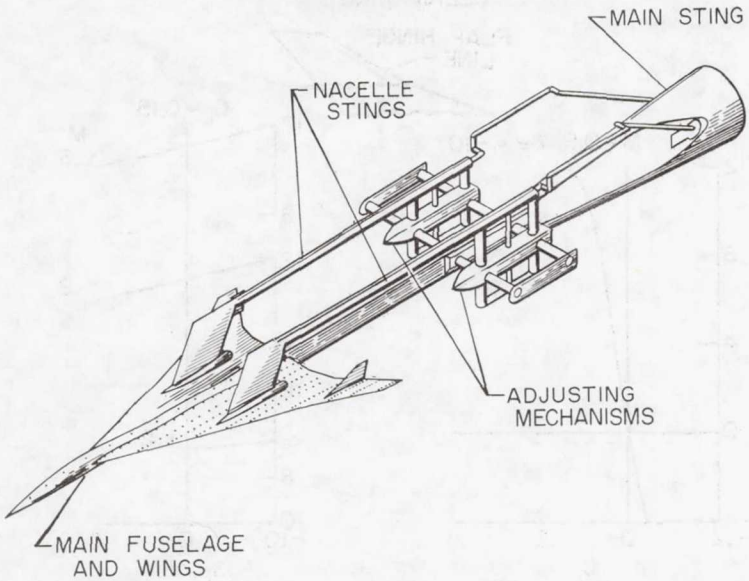

(a) SCAR model and air-powered sting system.

FRONT VIEW

JET NACELLE LOCATIONS

x/c	y/(b/2)	z/D_e
-0.170	0.462	2.04
.102	.462	2.04
.820	.462	2.04
.308	.249	2.04
-0.170	.462	2.04
-0.686	.580	2.04
-0.170	.462	2.25
-0.170	.462	2.04
0.170	.462	1.59

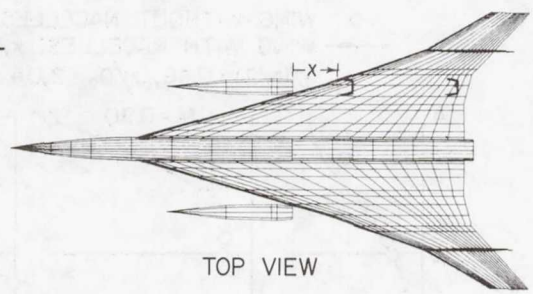

TOP VIEW

LEFT SIDE VIEW

(b) Computerized three-view sketch of model with jet nacelle locations.

Figure 2.- Sketches of model.

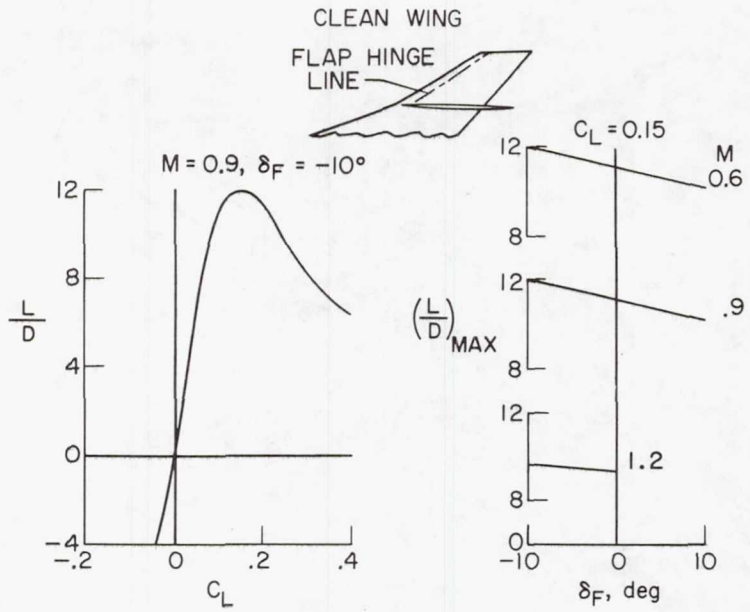

Figure 3.- Effects of deflection of wing tip leading edge flaps on lift to drag ratio.

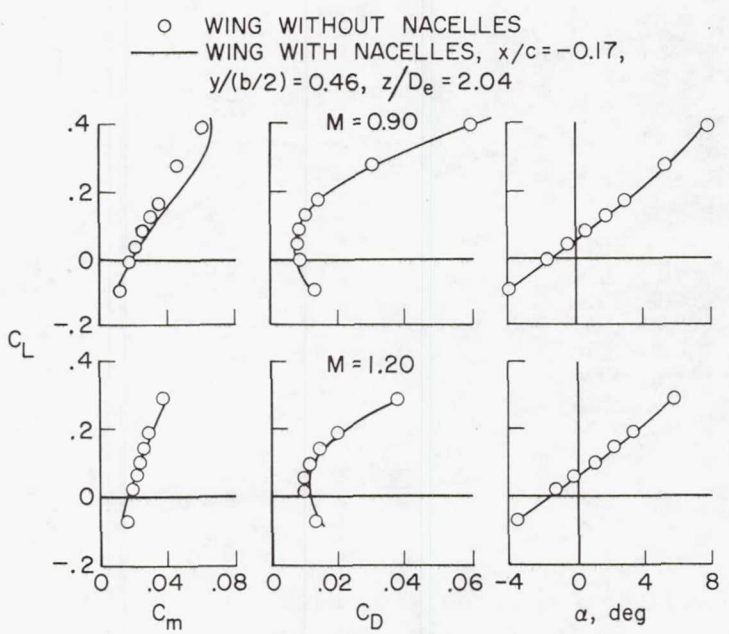

Figure 4.- Nacelle installation interference effects.

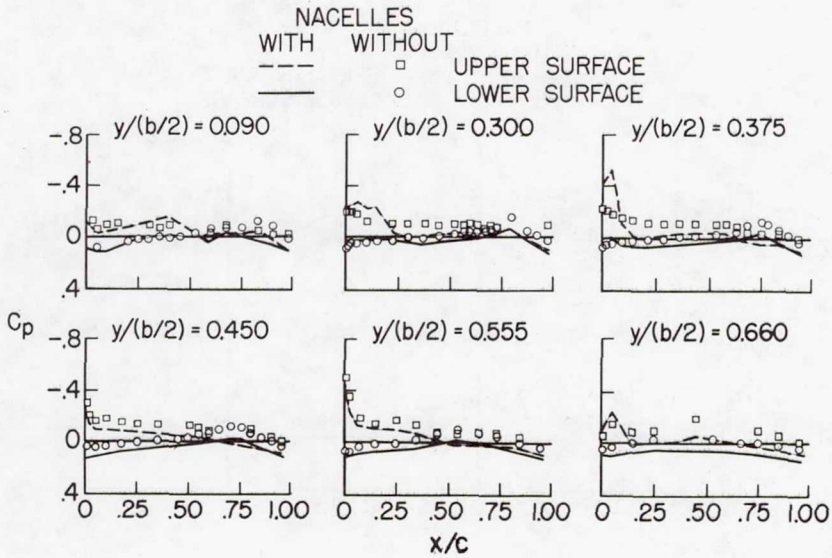

(a) M = 0.9; $\alpha = 0^{o}$.

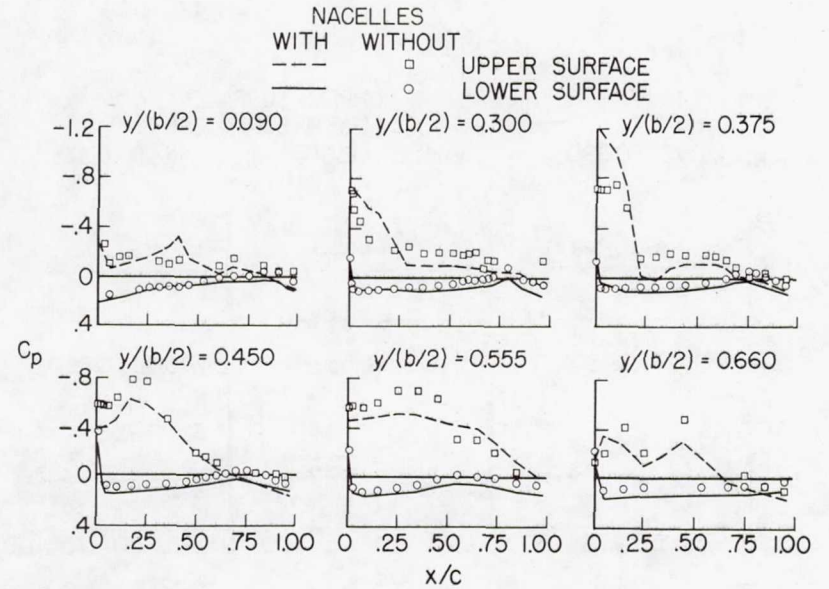

(b) M = 0.9; $\alpha = 4^{o}$.

Figure 5.- Typical wing pressure distributions with and without jet nacelles. x/c = -0.17; y/(b/2) = 0.46; z/D_e = 2.04.

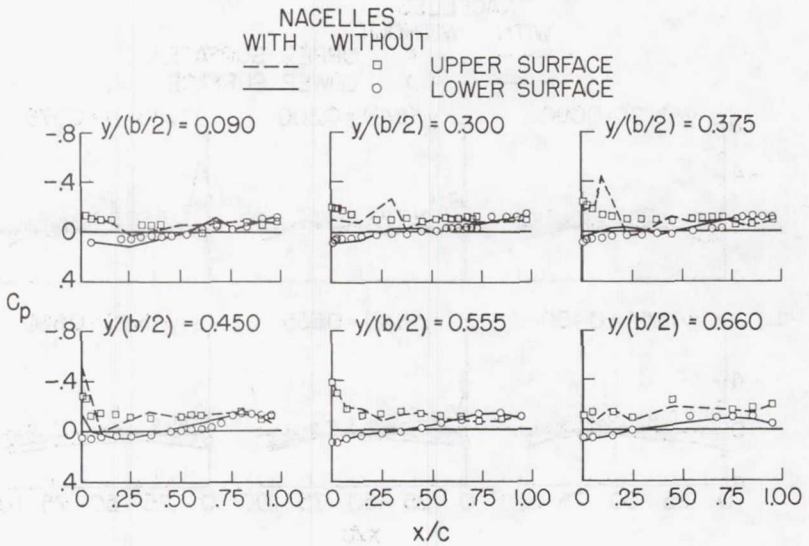

(c) M = 1.2; $\alpha = 0^{o}$.

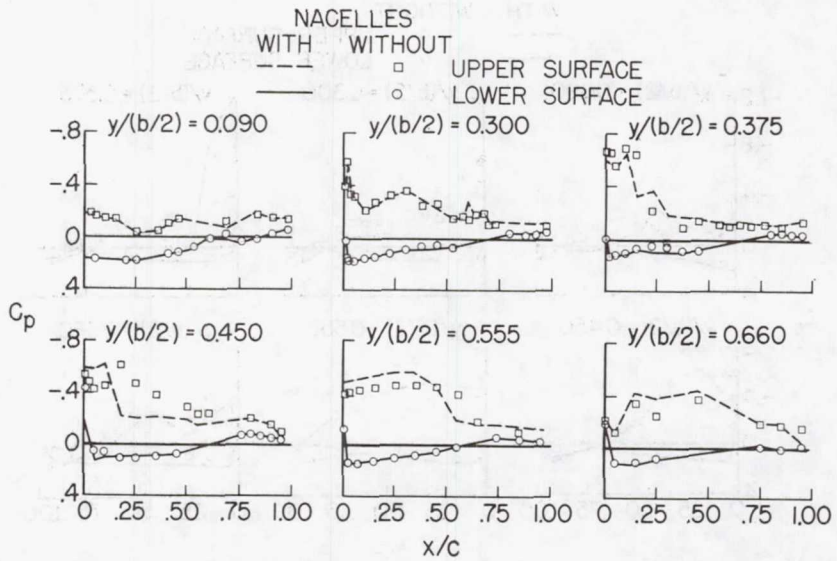

(d) M = 1.2; $\alpha = 4^{o}$.

Figure 5.- Concluded.

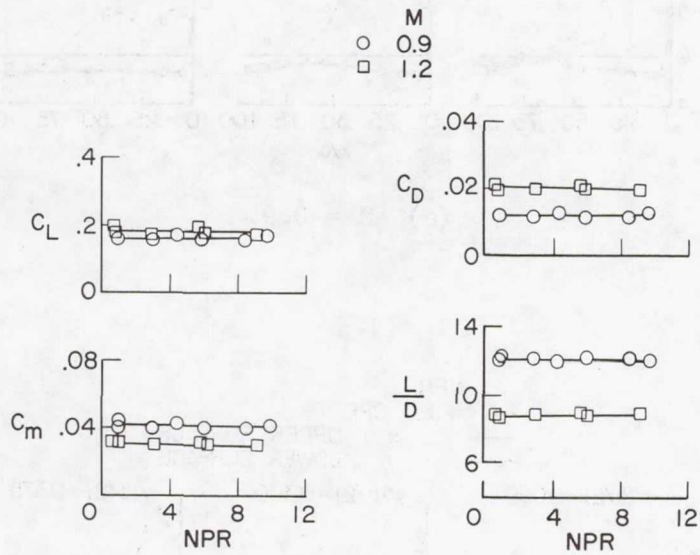

Figure 6.- Effect of jet exhaust flow variation on aerodynamic forces and moments. $\alpha \approx 3^{o}$; $x/c = -0.17$; $y/(b/2) = 0.46$; $z/D_e = 2.04$.

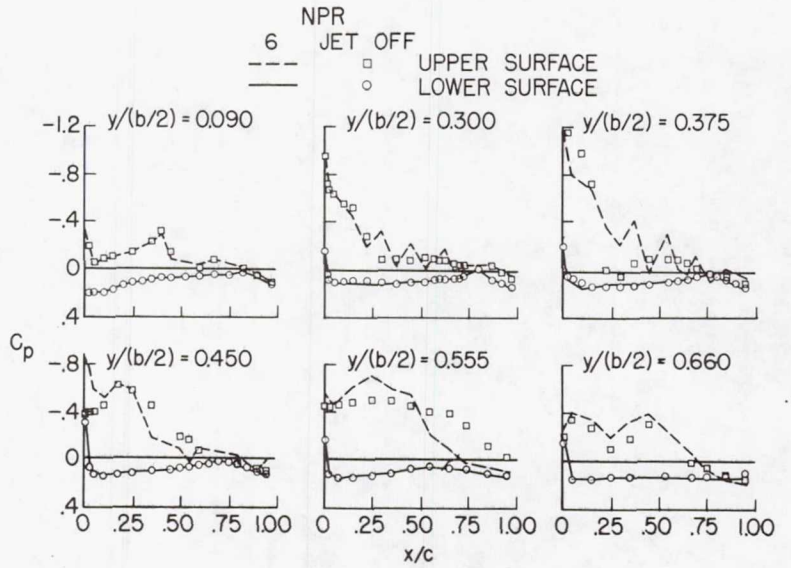

(a) M = 0.9.

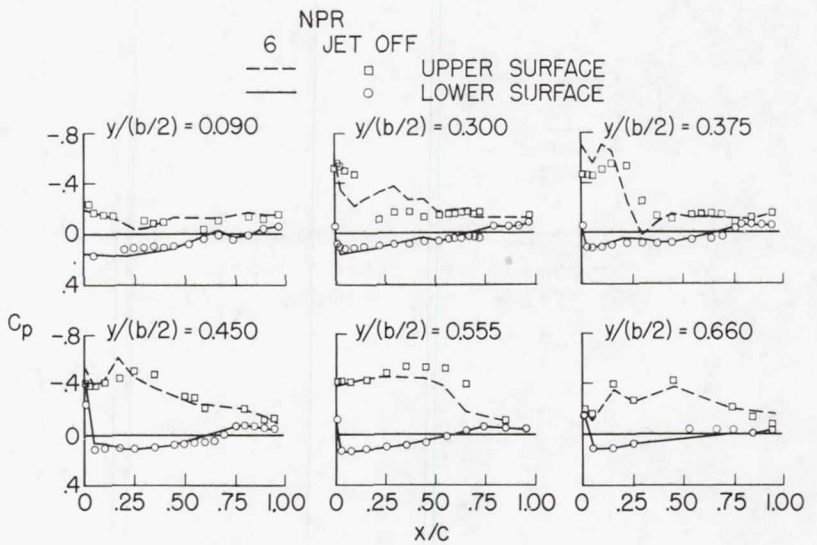

(b) M = 1.2.

Figure 7.- Effect of jet exhaust flow on wing pressure distributions. $\alpha = 4^{o}$; $x/c = -0.17$; $y/(b/2) = 0.46$; $z/D_e = 2.04$.

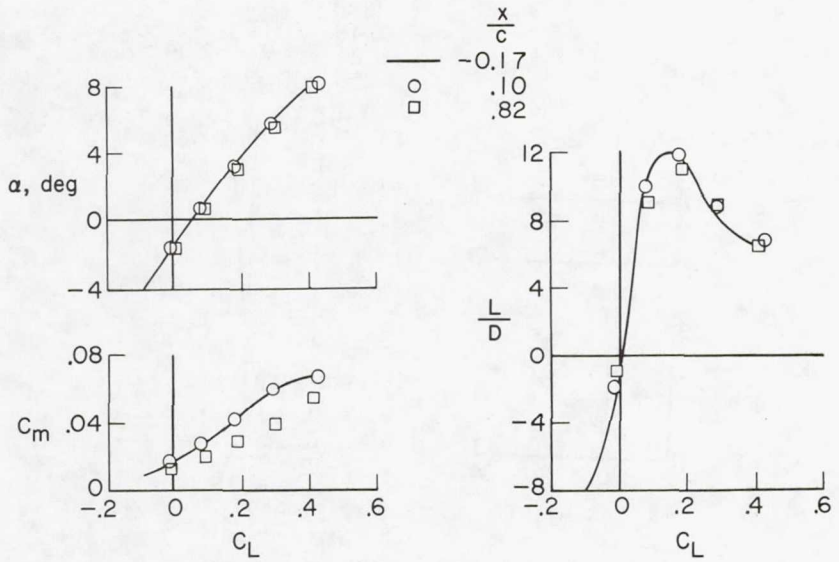

(a) M = 0.9; NPR = 4.6.

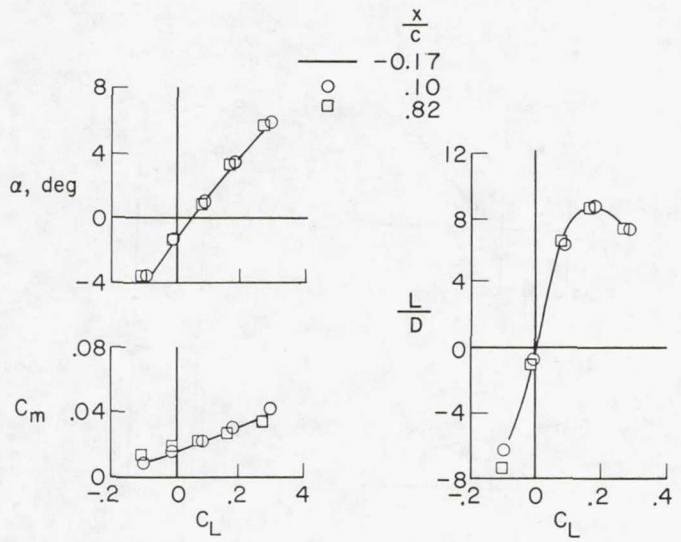

(b) M = 1.2; NPR = 8.0.

Figure 8.- Effect of nacelle chordwise location on longitudinal aerodynamic forces and moments. $y/(b/2) = 0.46$; $z/D_e = 2.04$.

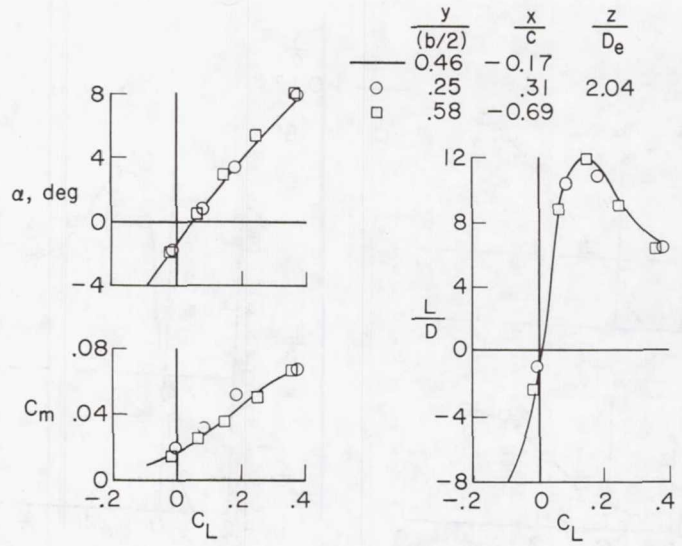

(a) M = 0.90; NPR = 4.6.

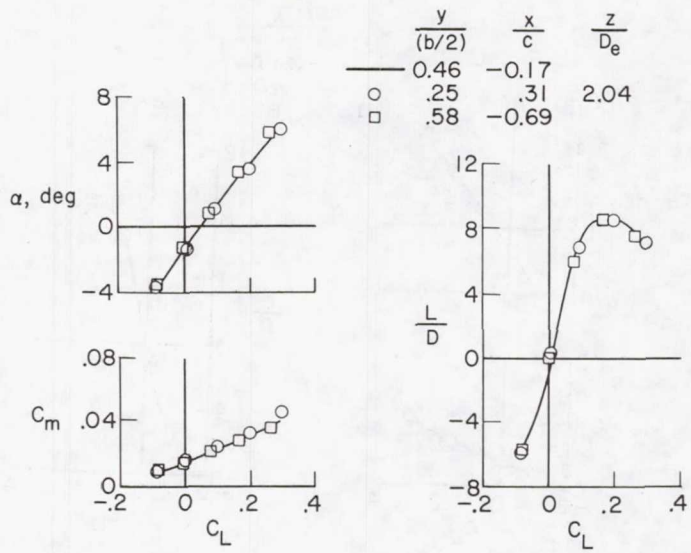

(b) M = 1.2; NPR = 8.0.

Figure. 9- Effect of nacelle spanwise position on aerodynamic forces and moments.

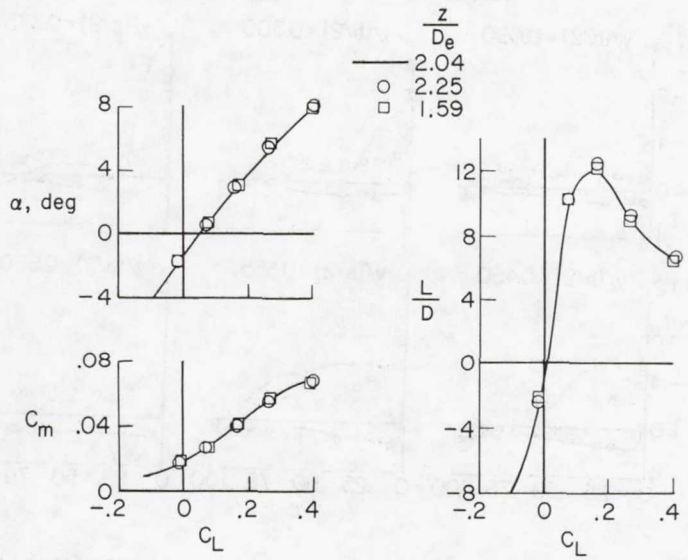

(a) M = 0.9; NPR = 4.6.

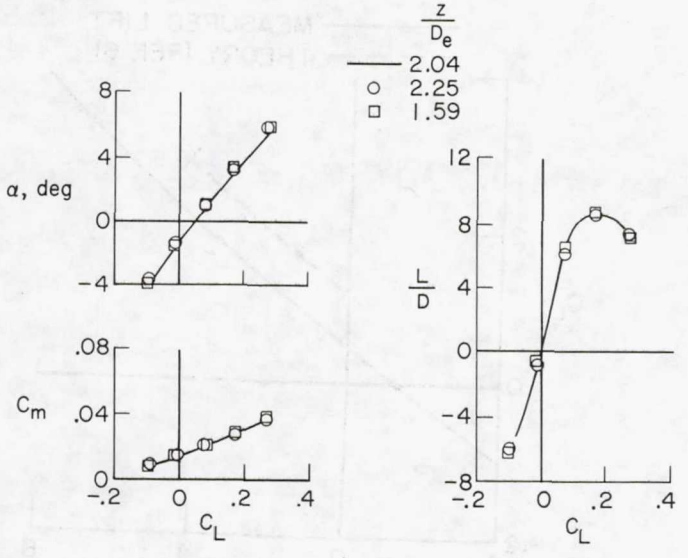

(b) M = 1.2; NPR = 8.0.

Figure 10.- Effect of vertical nacelle height variation on aerodynamic forces and moments. x/c = -0.17; y/(b/2) = 0.46.

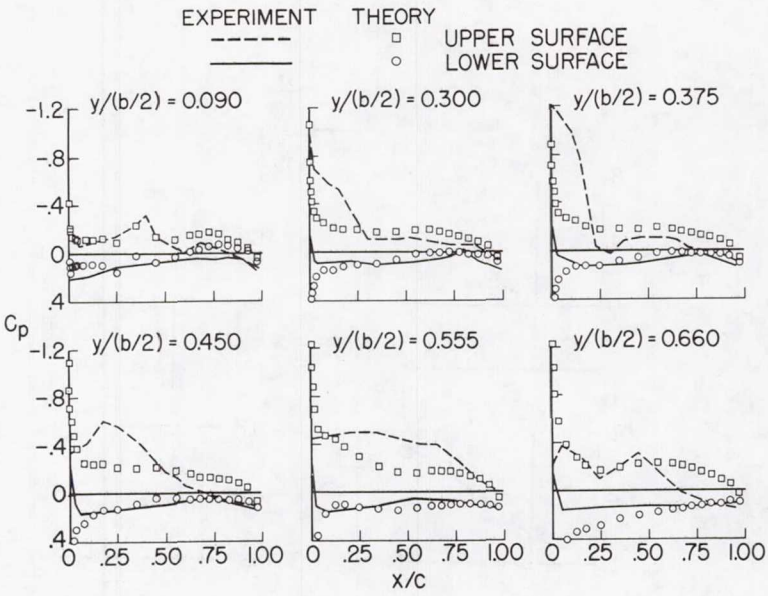

Figure 11.- Comparison between experimental pressure coefficients and theory of reference 6. M = 0.9; $\alpha = 4^{o}$; jet off; x/c = -0.17; $z/D_e = 2.04$.

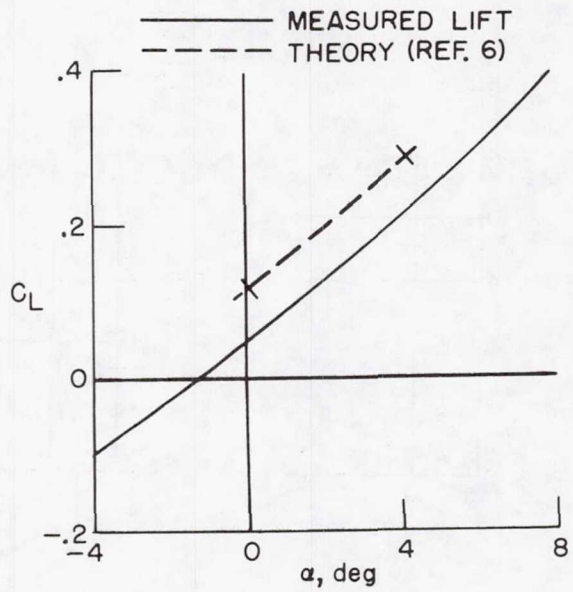

Figure 12.- Measured and predicted (ref. 6) wing-body lift coefficients. M = 0.9; x/c = -0.17; y/(b/2) = 0.46; $z/D_e = 2.04$.